Nonlinear thermal-distortion predictions of a silicon monochromator using the finite element method

Gordon Tajiri,[a] Wah-Keat Lee,[a]* Patricia Fernandez,[a] Dennis Mills,[a] Lahsen Assoufid[a] and Farid Amirouche[b]

[a]User Program Division, Advanced Photon Source, Argonne National Laboratory, Argonne, IL 60439, USA, and [b]Department of Mechanical Engineering, University of Illinois at Chicago, Chicago, IL 60607, USA. E-mail: wklee@aps.anl.gov

Silicon crystal monochromators at cryogenic temperatures have been used with great success at third-generation synchrotron radiation sources. At the Advanced Photon Source the unique characteristics of silicon at liquid nitrogen temperatures (80 K) have been leveraged to significantly reduce the thermally induced distortions on beamline monochromators. Finite element simulations of the nonlinear (temperature-dependent material properties) thermal stress problem were performed and compared with the experimental measurements. Several critical finite element modeling considerations are discussed for their role in accurately predicting the highly coupled thermal and structural response of the optical component's surface distortion to the high thermal heat flux. Once an understanding of the effects of (i) local element mesh size, (ii) area/surface heat flux *versus* volumetric heat generation, and (iii) uniform volumetric absorbed power *versus* a depth-dependent absorbed power, a final series of simulations was performed. Depending on the estimated convection heat-transfer coefficient, the final refined finite element model's predictions correlated well with the experimental measurements. In general, the use of the finite element method in predicting the overall thermal and structural behavior of the surface of the optical components with a high heat flux was shown to be quite effective.

Keywords: finite element method; silicon monochromators; nonlinear thermal distortions.

1. Introduction

Silicon crystal monochromators at cryogenic temperatures have been used with great success at third-generation synchrotron radiation sources (Rogers *et al.*, 1995; Lee *et al.*, 1995; Marot *et al.*, 1992, Marot, 1995). The thermal distortions of cryogenically cooled silicon crystal monochromators have been measured and characterized for various total incident powers and power densities by the Synchrotron Radiation Instrumentation Collaborative Access Team, SRICAT, at the Advanced Photon Source (APS) (Lee *et al.*, 2000). This experimental work has shown that localized distortion in the beam footprint is highly dependent on the characteristics of the beam and the incident angle, *e.g.* the distribution of the absorbed power as the beam travels through the crystal. To aid in the design of future optical components, a predictive tool/methodology needs to be developed that is able to (i) accurately model the complex/detailed design geometry and (ii) simulate and solve for nonuniform thermal loading and nonlinear material properties. *ANSYS*, a general purpose finite element analysis (FEA) code, was used to analyze and characterize the current silicon monochromator design used by the SRICAT.

Zhang (1993) has used a two-dimensional spatially dependent application of the thermal heat load as an area flux on the surface of the optical component to characterize the thermal distortion in the area of the beam's footprint. This loading assumes that all the energy is absorbed at or very near to the surface. Another approach, discussed by Assoufid *et al.* (1994), is to consider the loading as a distributed volumetric heat generation of the total power absorbed by the silicon crystal as the beam passes through the crystal. A comparison between a uniform surface heat flux, single uniform volumetric heat generation, and a layered/distributed volumetric loading needs to be analyzed and understood. The effects of these methods of thermal loading on (i) the peak temperature in the footprint of the beam, (ii) the local thermal gradients, and (iii) the mean temperature in the region local to the surface footprint of the beam must be characterized. From these results, a consistent methodology will be used in all subsequent FEA studies. *XOP* (Dejus & Rio, 1996), a computer simulation tool used to predict X-ray beam interaction with various materials and surfaces, was used to determine the amount of absorbed power at different distances below the surface of the silicon crystal. The results from this calculation for APS undulator A at 11 mm gap (k = 2.6, 500 μm Be window) and for a beam energy of 8 keV (θ = 14.3°) are given in Table 1 for a total normal incident power of 938 W. The predicted distribution of absorbed power from Table 1 reveals that a large percentage of the total absorbed power is absorbed in a region within 1.0 mm of the surface. An almost equal amount is absorbed at traversed depths greater that 1.0 mm from the surface. This confirms the need for a detailed depth-dependent method of thermal loading. Beam parameters used in the computer model are defined in Table 2

2. Procedure

The original APS cryo-cooled silicon monochromator design is shown in Fig. 1. Owing to the symmetry of the geometry of the silicon monochromator and the location of the thermal loading, a detailed

Table 1
Absorbed power per 1.0 mm traversed distance in silicon.

Layer	Power absorbed (W)	%
1	327.27	34.89
2	103.83	11.07
3	68.14	7.26
4	50.83	5.42
5	40.31	4.30
6	33.15	3.53
7	27.94	2.98
8	23.95	2.55
9	20.80	2.22
10	18.25	1.95
11	16.15	1.72
12	14.38	1.53
13	12.88	1.37
14	11.59	1.24
15	10.47	1.12
16	9.50	1.01
17	8.64	0.92
18	7.88	0.84
19	7.21	0.77
20	6.61	0.70

Table 2
1IDA undulator beam parameters.

Energy (keV)	Slit size (H × V) (mm)	Gap (mm)	Incident angle (°)
8	3 × 2	11	14.3

half-model was created. The normal location of the beam on the surface of the crystal is over the slot (Figs. 1 and 2). The depth of the slot is about half of the depth (z-direction) of the crystal. This slot was included to reduce the total absorbed energy of the beam in the monochromator by allowing more energy to be transmitted (Fig. 1). Computer simulations with the beam in this area of the surface are referred to as the thin-web or thin-section model. Models were also created with the beam on the thick section of the crystal. The location of the beam for these models is toward the upstream edge of the crystal (Fig. 2).

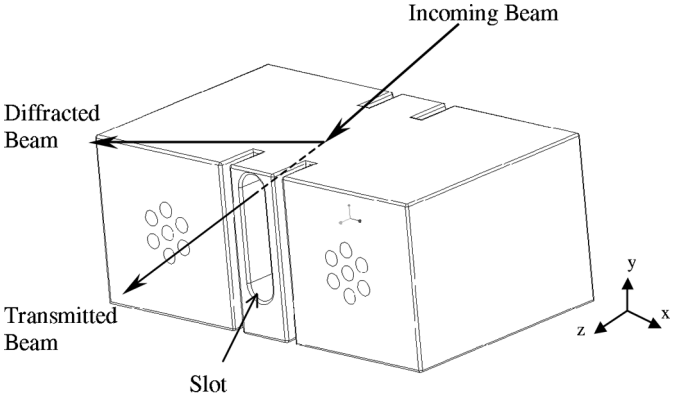

Figure 1
Silicon monochromator geometry and incident beam (x = 85 mm, y = 35 mm, z = 50 mm).

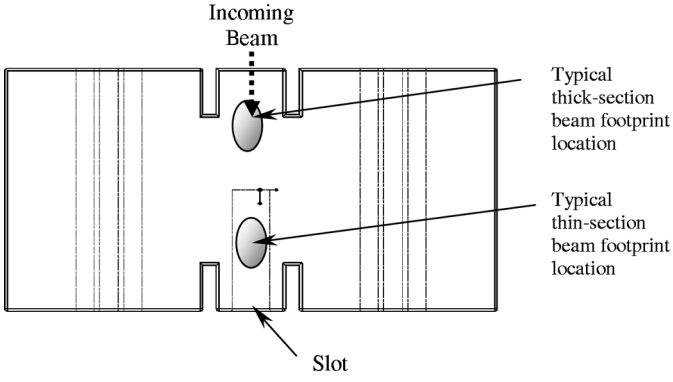

Figure 2
Silicon monochromator beam footprint locations (top view).

The assumptions for these simulations were as follows:

(1) Uniform or 'top-hat' spatial distribution of surface heat flux for area loading.

(2) Uniform heat generation (per layer if more than one volume is used) for volumetric loading.

(3) Half-model assumption owing to symmetry (*i.e.* 50% of total power simulated).

(4) Forced convection cooling at the surfaces of the coolant ports (all others adiabatic).

(5) Symmetry boundary conditions at the symmetry plane (zero x-displacement, zero z-moment).

(6) Mechanical constraints at seals to allow for expansion or contraction without rigid body motion.

2.1. *Study of coolant port geometry simplification*

In the initial model an attempt was made to exactly model the geometry of the seven individual 3.2 mm-diameter coolant ports and the rounded top and bottom surfaces of the slot. The six outer ports were equally spaced on a 9.5 mm diameter about a single center port. The detail required in modeling the seven individual coolant ports required a 'fine' finite element mesh (small elements) in that region (Fig. 3). This made the model large [33 782 elements, 101 346 degrees of freedom (DOF)] and difficult to solve. To reduce the computational time required to solve the full nonlinear thermal-stress problem, a simplified model with a single port was created and analyzed (Fig. 4). This simplified model has about one-third the number of elements (14 732 elements, 44 169 DOF). The diameter of the single port of the simplified model was made to be equal to the diagonal distance across the outer edges of the seven-port design (9.5 mm + 3.2 mm = 12.8 mm). This assumption is reasonable because the conductivity of silicon at 80 K is high (1340 W m^{-1} K^{-1}), and, as a consequence, this allows the individual ports to effectively work together in removing the heat. Additionally, this region was sufficiently far away from the high temperature gradients near and at the beam footprint.

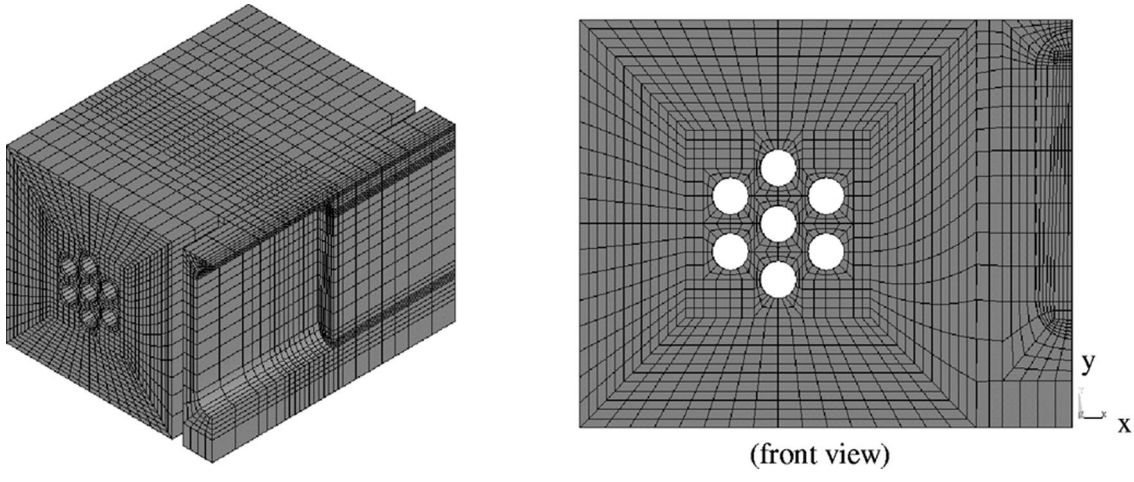

Figure 3
Detailed finite element half-model of the silicon monochromator.

Table 3
Convection coefficient comparison (liquid nitrogen material properties at 80 K).

Flow rate (l min^{-1}) (total)	Re	k (W m^{-1} K^{-1})	Pr	Nu_1 Equation (1)	h_1 (W m^{-2} K^{-1})	Nu_2 Equation (2)	h_2 (W m^{-2} K^{-1})
2.3	1.10×10^4	0.132	2.34	55.2	2280	56.3	2320
3.0	1.46×10^4	0.132	2.34	69.5	2870	72.5	2990
3.8	1.83×10^4	0.132	2.34	83.0	3430	87.9	3620
7.6	$\mathbf{3.66 \times 10^4}$	**0.132**	**2.34**	**145.0**	**5960**	**155.0**	**6380**
11.4	5.49×10^4	0.132	2.34	200.0	8250	219.0	9030
15.1	7.32×10^4	0.132	2.34	252.0	10400	280.0	11500
18.9	9.15×10^4	0.132	2.34	301.0	12400	337.0	13900
22.7	1.10×10^5	0.132	2.34	348.0	14400	393.0	16200

An important consideration in using this simplified model is the effective forced convection coefficient, $h_{\rm eff}$, that was used in the computer simulations. Since the surface area of the simplified single-port model was less than the combined total area of the actual seven individual ports, a correction factor, η, was used. The value of this correction factor is the ratio of the actual total area of the exact or detailed model to the area of the simplified model and was determined to be 1.7. The effective convection coefficient is then the product of the actual convection coefficient, h, and the correction factor, η. This is the convection coefficient used in the simplified model. In general, the forced convection coefficient, h or $h_{\rm eff}$, of the liquid nitrogen for a given flow rate through the actual multiple coolant port design or single simplified approximation were determined from the relationship

$$h = {\rm Nu}\, k/D$$

where Nu is the Nusselt number, $k = k(T)$ is the thermal conductivity of liquid nitrogen, and D is the hydraulic diameter of the port. The correlation for the Nusselt number for fully developed turbulent flow for a single-phase flow is most often given by the following equation (Incropera & Dewitt, 1981),

$$\mathrm{Nu} = 0.023\,\mathrm{Re}^{0.8}\,\mathrm{Pr}^{0.4}, \qquad (1)$$

where Re and Pr are the Reynold's and Prandtl numbers, respectively. A more accurate correlation formula, developed by Gnielinski (1993), is given as

$$\mathrm{Nu} = \frac{(f/2)(\mathrm{Re} - 10^3)\,\mathrm{Pr}}{1 + 12.7(f/2)^{1/2}(\mathrm{Pr}^{2/3} - 1)}, \qquad (2)$$

where f is the friction factor. Based on the Reynold's number, this factor for a smooth internal pipe is given by the following relationships,

$$f \cong 0.079\,\mathrm{Re}^{-1/4} \qquad 2 \times 10^3 < \mathrm{Re} < 2 \times 10^4,$$
$$f \cong 0.046\,\mathrm{Re}^{-1/5} \qquad 2 \times 10^4 < \mathrm{Re} < 10^6.$$

For closed channels with a surface finish other than smooth, the friction factor, f, is obtained from a Moody diagram. Evaluating these equations for liquid nitrogen at various flow rates, a comparison of the convection coefficient, h, from the two Nusselt number correlations was made. The results, as tabulated in Table 3, indicate that there is a slight difference between the Nusselt number (convection coefficient, h) correlations given by equations (1) and (2).

The previous empirical correlations for the convection coefficient are for single-phase fully developed turbulent flow. The complex flow path through the manifold and monochromator assembly is not accurately represented by the 'ideal' configurations used in determining these relationships. As an improvement for our crystal-to-manifold interface, we can include the effect of entrance configurations on single-phase, simultaneously developing velocity and temperature fields, which has been investigated by Molki (1987). Their experimental research has shown that the Nusselt number near the entrance at a distance x is given by the following relationship,

$$\frac{\mathrm{Nu}_{m,T}}{\mathrm{Nu}_\infty} = 1 + \frac{C}{(x/D)^n}, \qquad (3)$$

where $\mathrm{Nu}_{m,T}$ is the mean Nusselt number with a constant temperature wall condition, Nu_∞ is the fully developed turbulent-flow Nusselt number from equations (1) and (2), x is the distance from the

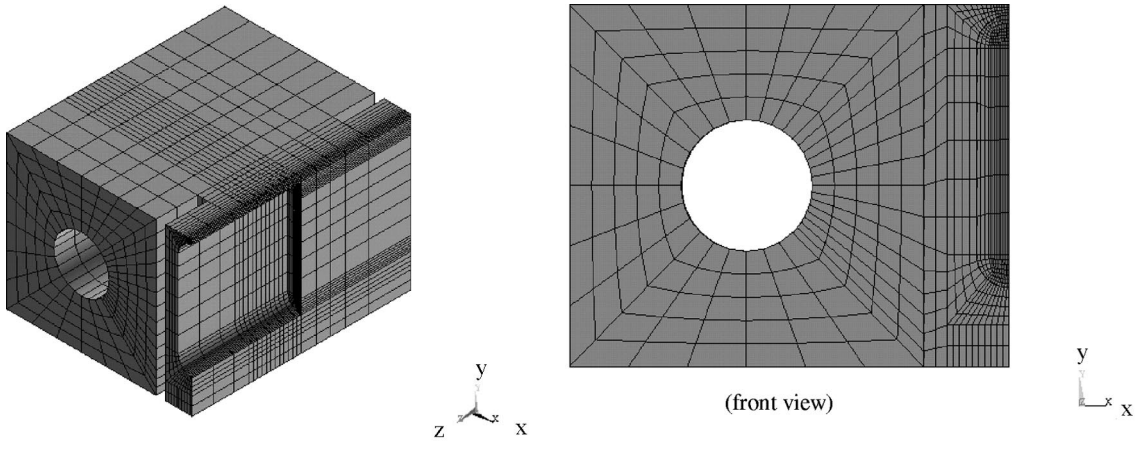

Figure 4
Simplified finite element half-model.

Table 4
Finite element model comparison.

Model	Maximum temperature (K)
Detailed with 7 ports	242.9
Simplified with 1 port	247.2

entrance, D is the diameter of the port, and the coefficients C and n are given below for a square entrance. Molki (1987) expressed these coefficients for a square entrance and Pr $\cong$ 2.5 as

$$C = 23.99\,\mathrm{Re}^{-0.230} \quad \text{and} \quad n = 0.815 - 2.08 \times 10^{-6}\,\mathrm{Re}.$$

In the current APS sector 1 monochromator design, the transition from the large single 13.5 mm-diameter port of the manifold to the seven smaller 3.2 mm-diameter ports of the silicon crystal is more accurately represented by this type of square entrance condition. Using the relationship given in equation (3) for single-phase, simultaneously developing turbulent flow with x at the center of the monochromator, the average convection heat-transfer coefficient is increased by about 50%. At distances near the entrance (<10 mm) the effect of the simultaneously developing flow is approximately 90%. The improved value for the Nusselt number for a flow rate of 7.0 l min^{-1} is found to be about 9000 W m^{-2} K^{-1}. A more accurate value must be determined empirically for this specific monochromator configuration. For this current study, upper and lower bounds for the convection coefficient were used and are 5000 to 20000 W m^{-2} K^{-1}, respectively.

The thermal and structural accuracy of the finite element model near and within the footprint of the beam, *i.e.* the region with the high thermal heat flux or heat generation, was negligibly affected by the above-described simplification of the finite element model. In the simplified model, the finite element mesh was allowed to be coarse in regions with slight temperature gradients, *e.g.* near the coolant ports. However, in the beam footprint and the material adjacent to it, *i.e.* regions with high temperature gradients, appropriately sized smaller elements were used. The local element size (x = 0.25 mm, y = 0.25 mm, z = 1.0 mm) in this region was identical in both models. A comparison of the peak temperatures within the footprint of the beam between these simulations indicated that there is a negligible loss in the accuracy (<2%) with the simplified model (Table 4). Consistent beam parameters, a single uniform volumetric heat-generation load of 550 W (275 W for the half-model) and a convection coefficient of 20000 W m^{-2} K^{-1} were used in both models.

As indicated from Table 4, the prediction of the simplified model is more conservative, *e.g.* the maximum temperature and associated thermal distortion will be slightly higher than that predicted by the detailed model. The loading parameters of the simplified model could be modified to exactly match the maximum temperature of the detailed model. However, for this analysis the slight conservatism of the simplified model in the predicted thermal response of the silicon crystal will be maintained.

2.2. *Study and comparison of different methods of thermal loading*

2.2.1. *Uniform surface area loading.* The respective total absorbed powers for the thin-section and thick-section models were consistent for all thermal loading methods and were 586 W and 650 W. In this study, a convection coefficient of 20000 W m^{-2} K^{-1} with the simplified single coolant-port geometry was used. A uniform surface heat flux is the simplest method of thermally loading the crystal. This type of load is a heat flux that is uniformly applied in the area of the beam's footprint. The units for this load are in W m^{-2}, where the total absorbed power is in watts W, and the area of the footprint is in meters squared, m^2. This method assumes that all the absorbed power is deposited at the surface of the crystal. Subsequently, the method will in general overpredict the maximum temperature and resulting thermal distortion. An energy balance of the model was performed to confirm the total absorbed.

2.2.2. *Single uniform volumetric loading.* Since the energy of the beam is absorbed as the beam travels through the crystal, a more realistic model would use a volumetric generation of the energy. A simplified model that included this volumetric absorption of energy was considered. This simplified volumetric model assumed a single uniform volumetric load. For the thin-section FEA model, this loading method assumed that the total absorbed power occurred uniformly in a volume directly beneath the footprint of the beam. An approximate rectangular volume with a varying thickness equal to the thin (1.2 mm minimum thickness) web above the crystal's slot and with a cross-sectional area equal to half of the beam's actual footprint, *i.e.* the assumption of symmetry, was used. For this simplified method of thermal loading, we assumed that all the absorbed power was uniformly generated within this volume. An energy balance of the heat-generating elements was performed to confirm the total absorbed power of the model.

2.2.3. *Discrete angle-dependent volumetric loading.* A more accurate representation of the thermal loading is achieved by breaking the single uniform volumetric load into multiple discrete volumes that are staggered to simulate the beam's path as it travels through the crystal. As mentioned above, *XOP* was used to determine the normal incident absorbed power in 1.0 mm increments along the path of the beam. In the finite element model, this corresponds to the distance from the surface of the crystal along the ($\theta = 14.3^\circ$) path of the beam. For elements in the beam footprint, an approximate element thickness of 0.26 to 0.24 mm was used. The results from the *XOP* calculation were then used as uniform volumetric thermal loads for each layer of the finite element model. The geometry assumed for the staggered elemental volumes is given in Fig. 5. An energy balance of the input elements was performed to confirm the total absorbed power of the model.

A summary of the results from the thin-section simulations for the various methods of power input is given in Table 5. In all cases the beam parameters are those given in Table 2, the convection coefficient was 20000 W m^{-2} K^{-1}, and the total absorbed power was 586 W. Maximum temperature and slope error were the parameters

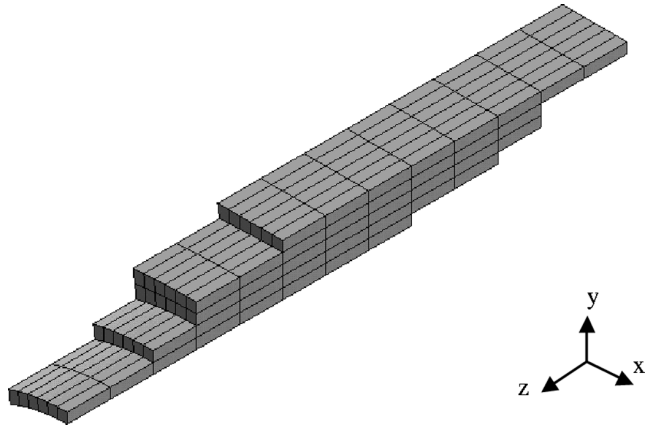

Figure 5
Volumetric heat generation in five discrete staggered layers (element size: 1.0 mm in z-direction, 0.25 mm in x-direction, 0.25 mm thick).

Table 5
Comparison of loading method on thin-section thermal distortion.

Thermal loading method	Maximum temperature (K)
Uniform surface heat flux	312.0
Single uniform heat generation	259.0
Staggered five-layer heat generation	262.0

Thermal loading method	Slope error (μrad)
Uniform surface heat flux	555.6
Single uniform heat generation	424.6
Staggered five-layer heat generation	420.8

Table 6
Comparison of loading method on thick-section thermal distortion.

Thermal loading method	Maximum temperature (K)
Single uniform heat generation	174.7
Staggered eight-layer heat generation	169.9

Thermal loading method	Slope error (μrad)
Single uniform heat generation	96.8
Staggered eight-layer heat generation	65.0

used to compare the results. A comparison of the magnitudes of these parameters reveals several differences in the thermal and structural response of the monochromator to the thermal loading method. The uniform *surface* heat flux method of loading resulted in the highest maximum temperature and an *overprediction* of the distortion in the footprint of the beam, due to the unrealistic concentration of the power at the surface. As shown in Table 5, the thin-section models of the single uniform volumetric load and the detailed staggered volumetric loads produced similar distortions. This result was unexpected since, for the case of the detailed staggered model with multiple layers, over 50% of the total absorbed power was dissipated in the first 0.24 mm-thick layer of the 1.2 mm web.

To better understand this apparent discrepancy, a similar comparison between single and multilayer volumetric thermal loading was performed for the *thick section* of the crystal. For the thick-section model, more element layers were needed to accurately simulate the path of the beam through the crystal. As shown in Figs. 2 and 6, with the beam centered over the thick section of the crystal the beam travels through more material. For this model and incident beam angle of 14.3°, the appropriate number of elemental layers was determined to be eight. A comparison of the results for these simulations is given in Table 6. As before, the convection coefficient was 20000 W m^{-2} K^{-1}, and the total absorbed power for the thick-section model was increased to 650 W.

Contrary to the thin-section model, the method of volumetric loading in the thick-section model made a significant difference in the predicted maximum thermal distortion and temperature (Tables 5 and 6). The reason for the difference, in the case of the thin-section or slotted model, is probably due to the lack of a 'good' thermal path under the elements with volumetric heat generation. Since the crystal is in a high-vacuum environment, no thermal energy (radiation heat transfer was not included in this analysis) is allowed to pass from the thin section into the slot. This boundary at the interface between the silicon material of the crystal and the slot is a perfectly insulated wall. As a consequence, the path of thermal energy removal (heat flow) is restricted. The effect of this restriction is to limit the spreading of thermal energy out from the volume of material directly beneath the footprint of the beam. As a consequence, the results from the single volumetric load and staggered five-layer load appear equivalent. However, in general, as seen in the thick-section analysis, this will not be the case. As a consequence, the method of using a single volumetric load cannot be used as a convenient simplification. Instead it is important that a model with discrete multilayer volumetric heat-generation loads be used. This was the method of thermal loading used in all subsequent simulations.

Table 7
Effect of local element size (E-size) on thermal distortion.

Thermal loading method	Maximum temperature (K)
Staggered five-layer, 0.5 mm E-size, heat generation	259.1
Staggered five-layer, 1.0 mm E-size, heat generation	262.0
Staggered five-layer, 2.0 mm E-size, heat generation	256.1

Thermal loading method	Slope error (μrad)
Staggered five-layer, 0.5 mm E-size, heat generation	422.3
Staggered five-layer, 1.0 mm E-size, heat generation	420.8
Staggered five-layer, 2.0 mm E-size, heat generation	325.5

2.3. *Study of local element size*

Local mesh size in the tangential direction (z-direction) in the footprint area of the beam was another parameter that was studied. The size of the elements in the z-direction of the beam was varied to determine its effect on the predicted slope error. Separate FEA models with local element sizes of 2.0, 1.0 and 0.5 mm were created and solved. The 1.0 mm case is the same model that was discussed in §2.2.3. The increased computational time required to solve problems with more (smaller) elements *versus* the accuracy of the results was considered, and a decision was made to determine an appropriate element size without a severe loss of accuracy of the results.

Table 7 contains a summary of the results from this investigation. The results indicate that larger elements that are greater than 2.0 mm in the area of the footprint of the beam significantly underpredict the thermal distortion, even though the predicted maximum temperature is consistent with models with smaller elements. This result is an indication of an increase in the model's local structural stiffness that is caused by a coarse local mesh. A reduction in the local element size from 1.0 mm to 0.5 mm showed only a slight change in the magnitude of the distortion.

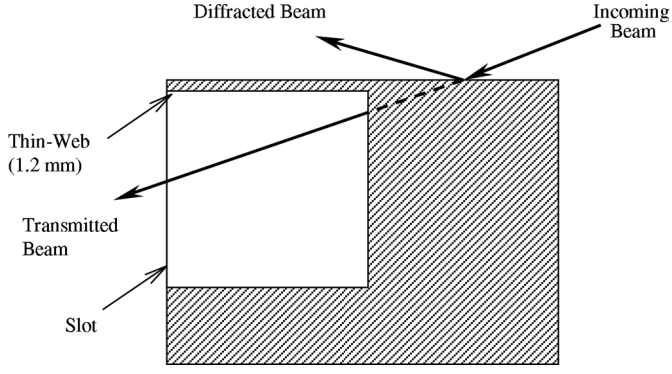

Figure 6
Monochromator cross section – thick-section beam detail (not to scale).

Depending on the geometry of the crystal and the method used to create the finite element model, a smaller local element size in the footprint of the beam will be translated throughout the model. As a result, the total number of elements for the model is significantly increased. This corresponds to an increase in the time required to solve the model. Subsequently, since the change in the predicted distortion (slope error) was less than 1% between the 0.5 and 1.0 mm local element sizes, the larger (1.0 mm) element will be used. This 1.0 mm local element size in the footprint of the beam and the discrete staggered method of thermal loading, as discussed above in §§2.2 and 2.3, were used in all subsequent simulations.

3. Analysis

3.1. *Simplified FEA model*

As discussed above, a simplified model with (i) a simplified geometry for the coolant ports, (ii) a local element size of 1.0 mm in the direction of the beam, and (iii) a discrete multilayer volumetric thermal loading method was used in studying the thermal distortion in the footprint of the beam. This model, with its reduced number of elements away from the beam's footprint and 'refined' elements in the beam's footprint (x = 0.25 mm, y = 0.24 mm, z = 1.0 mm), was a good compromise between computational solution time and accuracy of the results. The total absorbed power and the convection coefficient were varied and the thermal and structural response of the optical component in the footprint of the beam was characterized.

3.2. *Characterization of the thermal distortion*

Finite element models were created to study the effect of the convection cooling and monochromator geometry (comparison of thin section and thick section) on the maximum predicted temperature and slope error in the footprint of the beam. Performance limits of the current silicon monochromator design for a range of total absorbed powers were determined. As mentioned above, this design also included a slot to reduce the total absorbed power by reducing the material through which the beam travels. The effectiveness of the addition of this slot in reducing the thermal distortion was also considered.

As given in Table 2, a model was created to simulate a 3.0 mm (horizontal) $\times$ 2.0 mm (vertical) beam at 8 keV [Si(111), $\theta = 14.3^\circ$] with an APS undulator A at a closed gap of 11 mm. As discussed in §2.1 and given by equation (3) from that section, the best estimate of the forced convection coefficient for the current crystal design at the APS is for single-phase simultaneously developing turbulent flow. For a flow rate of 7.0 l min^{-1} the convection coefficient is approximated to be about 9000 W m^{-2} K^{-1}. Additionally, depending on the pressure of the liquid nitrogen within the crystal and the local temperatures at the walls of the coolant ports, two-phase cooling is possible. The presence of two-phase cooling would significantly increase the convection cooling coefficient. As a result, an accurate value for the convection coefficient for (i) the actual fluid flow geometry through the crystal and manifold and (ii) various flow rates must be determined experimentally. For these reasons a range of forced convection coefficients that bound this problem about 9000 W m^{-2} K^{-1} was used. For both the thin-section and thick-section models, the estimated range of the convection coefficient was from 5000 to 20000 W m^{-2} K^{-1}.

Thick-section and thin-section models with multilayer staggered thermal loading and a beam footprint element size of 1.0 mm in the z-direction were solved for temperature and vertical displacement (thermal distortion). Graphical results for temperature and surface displacement for the thin-section solution are given in Figs. 7 and 8, respectively. For a beam footprint in the thin section of the crystal, the high temperature gradients in and near the footprint are apparent from Fig. 7. The 'thermal bump', caused by these highly localized thermal gradients and silicon's highly temperature-dependent coefficient of thermal expansion, is clearly shown in Fig. 8 in the footprint of the beam. The worst-case maximum slope error of the distortion within the footprint of the beam is taken along this plane of symmetry, *i.e.* the center of the beam.

The slope error was calculated from the vertical displacements of the nodes along the center of the beam. For a given total absorbed power, this is the location of the maximum surface distortion. A family of constant convection coefficient curves, comparing the maximum thermal distortions for a range of absorbed powers, is shown in Fig. 9.

The total absorbed powers and corresponding depth-dependent distributions of power as used in these computer simulations are based on the assumption that for a given beam energy the depth-dependent distribution of absorbed power is proportionally constant for different storage-ring currents. The proportional distributions of absorbed power for the thin-section and thick-section models with the beam properties from Table 2 and a ring current of 100 mA were used as the basis for the approximated distribution of power for the models with different total absorbed powers, *e.g.* ring currents. As discussed above, *XOP* was used to simulate the total absorbed power and depth-dependent distribution of power at a ring current of 100 mA (Table 1). Fig. 9 clearly shows (i) the performance difference between the thick section and thin section and (ii) the effect of the convection coefficient. Based on an allowable distortion (slope error), the limits for the total absorbed power can be determined from these curves. With the beam on the thin section of the monochromator, the surface is relatively insensitive to the total absorbed power until about 250 to 300 W. Total absorbed powers above this value will cause a thermal distortion that increases rapidly with each incremental increase in total absorbed power. For a beam on the thick section, the surface in the footprint of the beam remains undistorted to about 450 W of total absorbed power. This significant difference is an indication that a good conductive thermal path (thermal conductivity of silicon at 80 K $\simeq$ 1340 W m^{-1} K^{-1}), to dissipate and spread the absorbed thermal power, is more effective in minimizing the thermal distortion than the addition of the slot. Additionally, as indicated above in Table 1, most of the absorbed power at normal incidence occurs in the first several millimeters as the beam travels through the silicon. Depending on the incident angle, θ, this corresponds to a few tenths of a millimeter below the surface. As a consequence, since the majority of the absorption of thermal power occurs near the surface, the benefit of the addition of the slot is further minimized. A comparison of the curves in Fig. 9 also shows the effect of the convection coefficient, which becomes increasingly more significant at higher absorbed powers, *i.e.* the vertical difference between the constant convection coefficient curves for a given beam location increases exponentially.

Although a few experimental data points [high-order high-energy (higher-harmonic) double-crystal rocking-curve widths] have been included in Fig. 9, comparisons between the FEA results and the experimental data should be taken with great caution for the following reasons:

(1) The FEA slope-error predictions presented in Fig. 9 are those along the crystal symmetry centerline and are thus the maximum tangential slope errors on the entire crystal surface. Experimentally, however, the data points reflect weighted averages of the slope errors over the entire beam footprint. Figs. 10 and 11 are plots of the change in the tangential slope error as a function of the distance from the

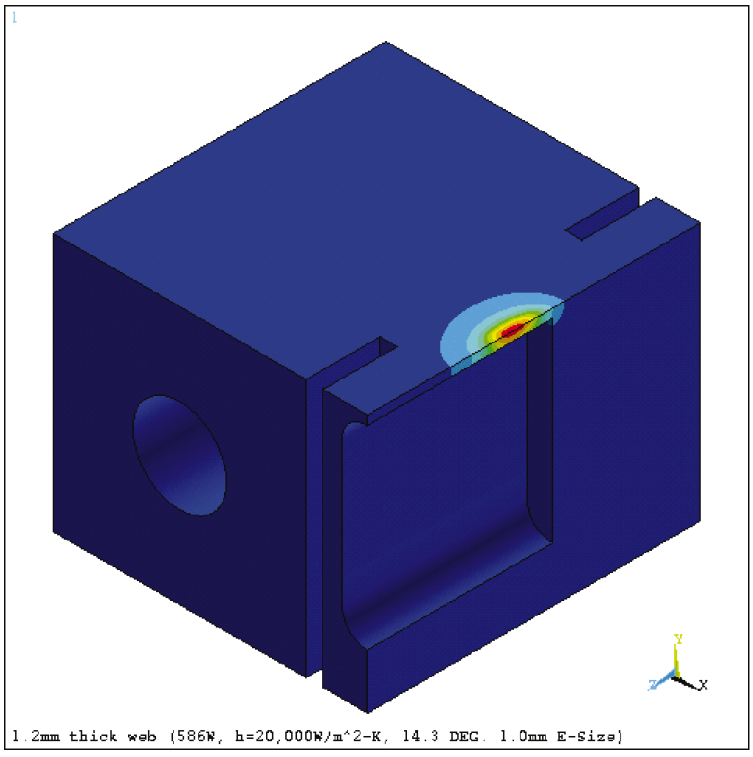

Figure 7
Thin-section model – temperature distribution.

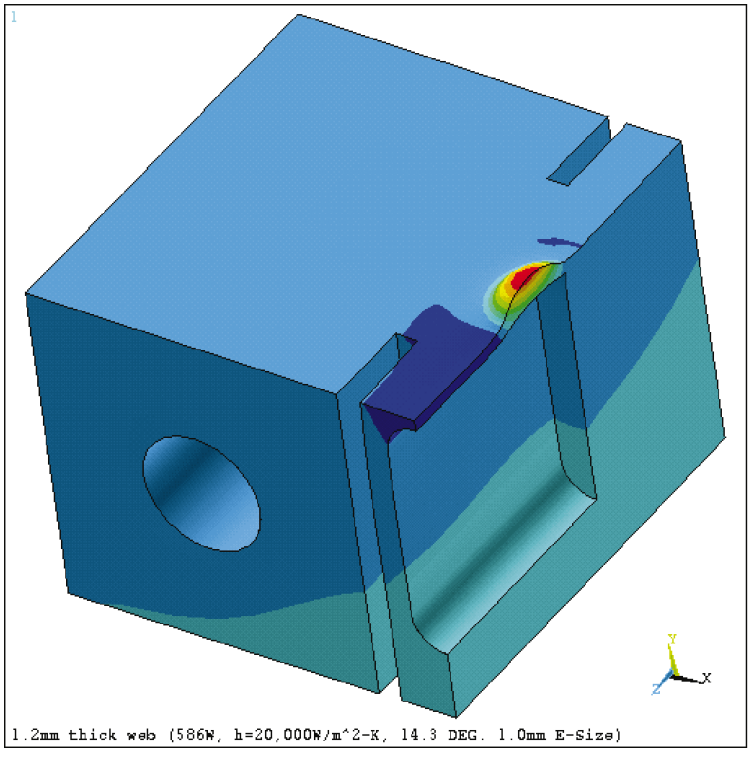

Figure 8
Thin-section model – vertical displacements.

centerline of the crystal, *i.e.* the center of the beam's footprint. The total absorbed powers for the thin-section and thick-section models were 450 W and 550 W, respectively. The convection coefficient used in both models was 20000 W m^{-2} K^{-1}. Figs. 10 and 11 clearly show that the slope error decreases for increased distances from the center of the beam. Thus, the FEA results in Fig. 9 should overestimate the experimental data.

(2) For a rigorous quantitative comparison, calculations using distorted crystal (Takagi–Taupin) dynamical diffraction theory, using the FEA results as input, must be performed (Freund *et al.*, 2000). Investigations using this approach are currently being pursued.

(3) Owing to residual crystal mounting-induced strains, experimental data points with rocking-curve widths of less than about 10 µrad do not accurately measure the thermal-induced slope errors.

The exact magnitude of the simulated distortion is highly dependent on the actual power absorbed by the crystal and the actual convection heat-transfer coefficient. As the absorbed power increases, the rate of change of the distortion increases significantly until a runaway condition occurs for powers greater than about 350 W for the thin section and, to a lesser degree, about 550 W for the thick section. This runaway condition of the thermal distortion is related to the temperature dependence of the $\alpha/k(T)$ ratio for silicon (Fig. 12). In this ratio, $\alpha(T)$ is the temperature-dependent coefficient of thermal expansion and $k(T)$ is the temperature-dependent thermal conductivity of silicon. For local temperatures within the footprint of the beam above about 130 K, this ratio, which is proportional to the distortion, exhibits a significant increase for slight increases in temperature.

4. Conclusions

The ability to model the actual geometry and a nonlinear finite element solver are necessary to accurately predict the thermal distortion on the surface of high-heat-flux optical components. Additionally, an accurate method of power input to the model and an optimal local element size need to be determined. In the present work, a sensitivity study based on these parameters was performed. The results indicate that the peak temperature and thermal distortion were affected by the method of thermal input to the model. Results show that a depth-dependent volumetric absorbed power generation is important in accurately predicting the thermal distortion of the

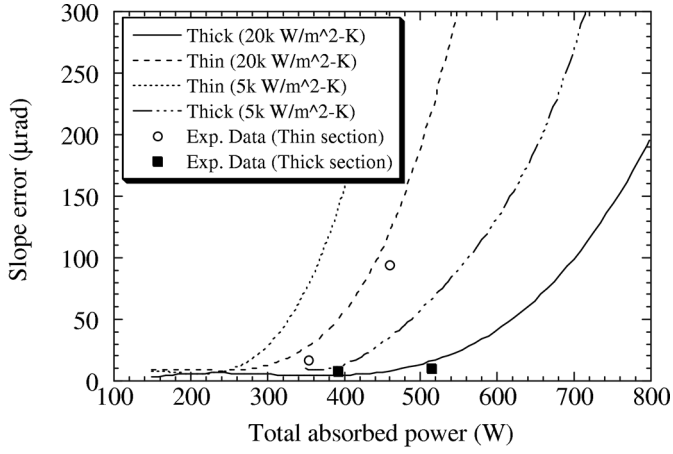

Figure 9
Comparison of thick-section and thin-section thermal distortions.

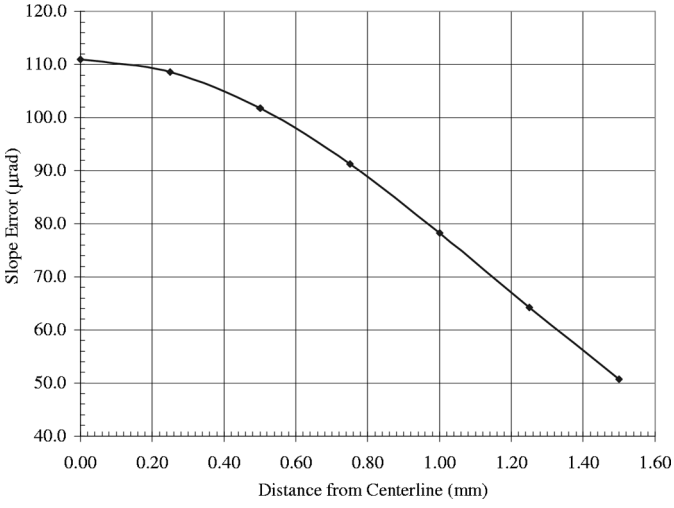

Figure 10
Thin-section beam footprint tangential slope error.

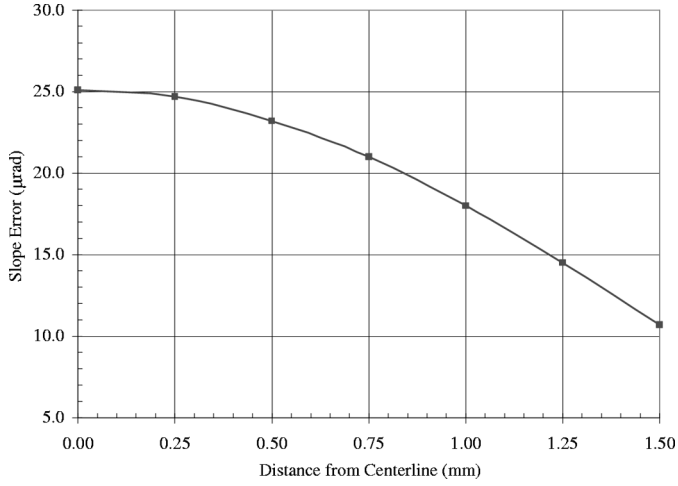

Figure 11
Thick-section beam footprint tangential slope error.

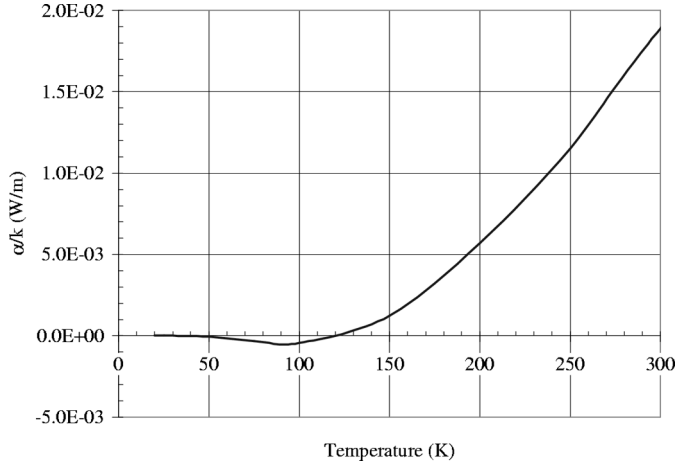

Figure 12
Temperature dependence of α/k.

monochromator's surface. The predicted maximum temperature in the footprint of the beam was negligibly affected by the element size. However, the element size did affect the magnitude of the distortion. Going from a 2 mm to 1 mm element length (tangential direction) resulted in predicted distortions that are about 12% higher. A further reduction in the element size from 1 mm to 0.5 mm resulted in only a slight increase of less than 2%. This inaccuracy is attributed to the local increase in stiffness of a finite element model with structural elements with aspect ratios that are too large. Depending on the assumed convection heat-transfer coefficient, the predicted thermal distortions caused by the absorbed power from the beam were consistent with those measured at the APS. The exact convection heat-transfer coefficient for this specific application must be experimentally quantified. Based on the experimental measurements and the FEA predictions, this value should be close to 20 000 W m^{-2} K^{-1}. Nonetheless, as a predictive tool for future high-heat-load optical designs, the methodology and techniques used in this work are reliable for estimating the thermal and structural response of the optical components for a given total absorbed power and power density. The results also indicate that at higher absorbed powers further reductions in the thermal distortion may be possible with enhancements that increase the convection heat-transfer coefficient (Kuzay, 1992).

This research is supported by the US Department of Energy, BES-Material Science, under Contract No. W-31-109-ENG-38.

References

Assoufid, L., Lee, W.-K. & Mills, D. M. (1994). Argonne National Laboratory report ANL/APS/TB-19. ANL, APS, Argonne, IL 60439, USA.
Dejus, R. J. & del Rio, M. S. (1996). *Rev. Sci. Instrum.* **67**. CD-ROM.
Freund, A. K., Hoszowska, J., Magliore, J.-S., Mocella, V., Zhang, L. & Ferrero, C. (2000). *Proceedings of SRI99: Eleventh US National Conference*, Stanford, California 1999, edited by P. Pianetta, J. Arthur & S. Brennan. Melville, NY: American Institute of Physics.

Gnielinski, V. (1993). *Heat Transfer*, pp. 312–317. New York: John Wiley.
Incropera, F. P. & Dewitt, D. P. (1981). *Fundamentals of Heat Transfer*, pp. 406–407. New York: John Wiley.
Kuzay, T. (1992). *Rev. Sci. Instrum.* **63**(1), 468–472.
Lee, W.-K., Fernandez, P. & Mills, D. M. (2000). *J. Synchrotron Rad.* **7**, 12–17.
Lee, W.-K., Mills, D. M., Assoufid, L., Blasdell, R. C., Fernandez, P. B., Rogers, C. S. & Smither, R. K. (1995). *Opt. Eng.* **34**, 418–425.
Marot, G. (1995). *Opt. Eng.* **34**, 426–431.
Marot, G., Rossat, M., Freund, A. & Berman, L. (1992). *Rev. Sci. Instrum.* **63**(1), 477–480.
Molki, M. (1987). *Handbook of Single-Phase Convection Heat Transfer*, ch. 4, pp. 4.55–4.59. New York: John Wiley.
Rogers, C. S., Mills, D. M., Lee, W.-K., Knapp, G. S., Holmberg, J., Freund, A., Wulff, M., Rossat, M., Hanfland, M. & Yamaoka, H. (1995). *Rev. Sci. Instrum.* **66**(6), 3494–3499.
Zhang, L. (1993). *Proc. SPIE*, **1997**, 223–235.